# Magnetic Phase Transition and Spin Wave Excitations in the Colossal Magnetoresistive Manganites: An Experiment Using the BT7 Triple-Axis Spectrometer

Yang Zhao, Guangyong Xu, William Ratcliff, and Jeffrey Lynn
NIST Center for Neutron Research

**OBJECTIVES:** The Spectroscopy school participants will use elastic scattering to measure the ferromagnetic order parameter and transition temperature, and inelastic neutron scattering measurements to study the spin wave excitations in the perovskite $La_{0.7}Sr_{0.3}MnO_3$. This system will allow us to demonstrate the versatility and power of triple-axis spectrometry in studying the static and dynamic properties of condensed matter systems.

## I. Introduction to the system

The improved modern-day material synthesis techniques for oxide materials were developed in part by the quest to fabricate high temperature superconductors, and has enabled researchers to revisit other systems such as the $LaMnO_3$ class of materials. The crystal structure of these materials is based on the cubic perovskite system, where the Mn ion is surrounded by six oxygen ions with octahedral symmetry, with the La ions on a simple cubic lattice as shown in Fig. 1. $LaMnO_3$ is an antiferromagnetic insulator ($T_N$=140 K), but the properties can be changed by substituting 2+ cations such as Ca, Sr, and Ba for $La^{3+}$. Doping $La_{1-x}A_xMnO_3$ in the range $0.2<x<0.5$ produces an isotropic, metallic ferromagnet at low temperature. The magnetic ordering (Curie) temperature is accompanied by a metal-insulator transition, which can then be controlled by the application of a magnetic field. The effect on the resistivity can be enormous—several orders-of-magnitude—which would be ideal for device applications such as for sensors and for read/write heads in magnetic storage media, where information is stored in the form of bits which are read by magnetic read heads. These magnetic read/write heads work by exhibiting a small change in their electrical resistivity as they pass over a magnetic bit. This change in the resistivity when the magnetic field changes is called magnetoresistance (MR) and materials evincing it are called magnetoresistive. Most materials have negligible MR, while the magnetoresistance is typically only a few percent in select metals and semiconductors. One favorable material is Permalloy, an alloy of iron and nickel, and this material was used for many years as read/write heads in disk media. The current generation of read/write heads in hard drives is based on multilayer thin film technology, which amplifies the magnetoresistive effect (≈20 %) and is termed giant magnetoresistance (GMR). The manganites, on the other hand, possess colossal magnetoresistance (CMR), as compared to the much smaller MR or GMR observed previously.

The basic physics behind this colossal change in resistivity is this insulator-to-metal transition, which often is first-order in nature and results in electronic phase separation (in which two electronic phases are spatially distinct) between ferromagnetic metallic and paramagnetic insulating states. The particular material that we will examine is $La_{0.7}Sr_{0.3}MnO_3$, where doped holes induce ferromagnetism and metallic conductivity. Let us first briefly discuss how doping the system leads to metallic conductivity [1].

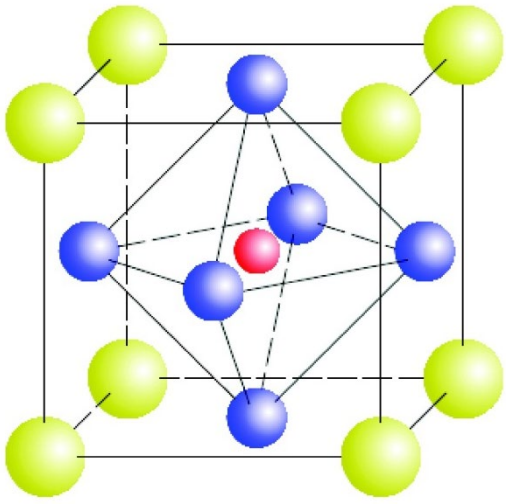

Fig. 1. A unit cell of a cubic perovskite $ABO_3$ structure The yellow, red, and blue spheres are La, Mn, and O sites, respectively.

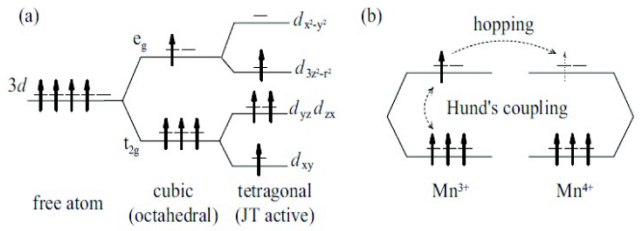


Fig. 2. (a) Cubic and tetragonal crystal field splitting of 3d orbitals of $Mn^{3+}$. (b) A simple representation of ferromagnetic coupling via double exchange.

In a crystal, the wave functions of electrons on neighboring atoms mix and their energy levels expand into bands of allowed energies. Because electrons follow the Pauli Exclusion principle, they cannot occupy the same states simultaneously. Thus, the electrons fill the available states up to an energy known as the Fermi energy, $E_F$. In metals, electrons near $E_F$ are still free to move because there are unoccupied states available in the band. An insulator (like $LaMnO_3$) is the case when all the available states are filled with electrons.

The manganites of interest here have crystal structures derived from cubic perovskite lattices (see Fig. 1), in which each Mn cation is surrounded by six oxygen ions which form an octahedron around it. For $La^{3+}Mn^{3+}O^{-2}{}_3$, the $Mn^{3+}$ ion has four d-electrons. In this cubic crystal environment, the energy levels of the d-electrons split into three degenerate orbitals (designated $t_{2g}$) and two degenerate $e_g$ orbitals, as shown in Fig. 2(a). Strong Hund's rule coupling (related to the minimization of Coulomb repulsion of the electrons on a given atom, while satisfying the Pauli exclusion principle) results in the spins of the 3d electrons needing to be aligned. As a result, three electrons with parallel spins occupy the lowest lying $t_{2g}$ orbitals, and form a localized magnetic moment with S=3/2. The fourth electron occupies the doubly degenerate $e_g$ level. This electron must also have its spin aligned with the spins in the $t_{2g}$ orbitals because of the same strong Hund's rule coupling. There are still six d orbitals that are unoccupied—another 3 $t_{2g}$ orbitals and two $e_g$ orbitals where the spins would be in the reverse direction, but these are very high in energy (compared to the thermal energies kT of interest) because of the strong Hund's rule coupling and are out of the picture.

Note that the occupied $e_g$ is doubly degenerate, which makes $Mn^{3+}$ a Jahn-Teller (JT) active ion. That is, the system may be able to lower its energy by allowing a distortion of the oxygen environment. Such a distortion breaks the degeneracy of the $e_g$ orbitals, with one orbital becoming lower in energy and the other higher than in the degenerate case (Fig. 2(a)). Since there is only one electron occupying the $e_g$ level, it can always lower its energy (at the cost of the elastic energy of the distortion). Therefore all these $Mn^{3+}$ oxides exhibit small distortions away from the ideal cubic structure, but are still insulating.

As we replace $La^{3+}$ cations with $Sr^{2+}$ cations, we change some of the $Mn^{3+}$ ions into $Mn^{4+}$ ions, where the $e_g$ orbital is unoccupied. This allows the $e_g$ electrons the possibility to hop to an adjacent unoccupied site (Fig. 2(b)). As the carrier concentration is varied, the system's physical properties change as shown in Fig. 3 [2]. The ferromagnetic order and metallic conductivity first show up at $x\approx0.1$ and at $x\approx0.15$, respectively. When the Sr concentration reaches $x\approx0.3$, the ferromagnetic transition temperature, $T_C$, becomes maximum and the system is a good metal.

Now, we've suggested how the system becomes metallic with doping, but the question remains, why does it become ferromagnetic (that is, why do the spins on different Mn sites spontaneously align in the same direction?). While there are various causes of magnetism in materials, the dominant factor for the manganites is known as double exchange. Here, there is a "virtual process" in which the $e_g$ electrons are allowed to hop from site to site through an oxygen orbital. If you imagine that the $e_g$ electron is hoping from an occupied $Mn^{3+}$ site to an unoccupied

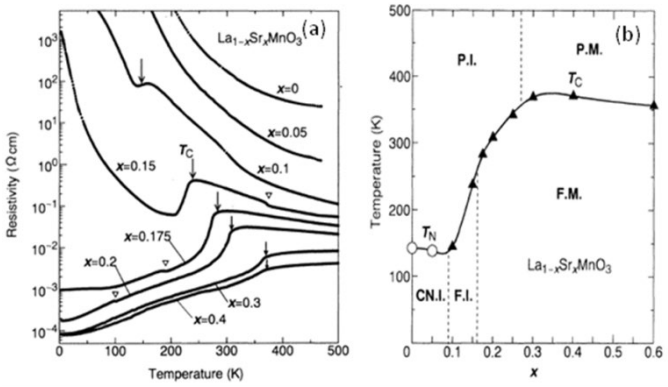


Fig. 3. (a) Resistivity of $La_{1-x}Sr_xMnO_3$ as a function of temperature. The arrows indicate critical temperatures for magnetic transitions. (b) The phase diagram of the $La_{1-x}Sr_xMnO_3$ system. The abbreviations F, P, CN, M, and I stand for ferromagnetic, paramagnetic, spin-canted antiferromagnetic, metallic and insulating, respectively [2].

$Mn^{4+}$ site, and back again, the probability of hoping will depend on the relative orientation of spins on the two sites (see Fig. 2(b)). In fact, because of the strong Hund's rule coupling, as the spin moves from the $Mn^{3+}$ site to the $Mn^{4+}$ site, it must be aligned with the $t_{2g}$ "core" spins on both sites. Therefore ferromagnetism evolves from the system by maximizing the probability of hopping. This is the physical basis behind the double-exchange model for the manganites.

*Question: (1) Based on the picture described in Fig.3, explain how magnetic field reduces the resistivity in CMR materials. (2) In Fig. 3(b), what would you suggest is the hole doping concentration that is potentially useful for a CMR read/write head application, and why?*

## II. THE BT-7 TRIPLE-AXIS SPECTROMETER

The basics of neutron scattering and the flexibility of a triple-axis spectrometer is covered in a separate experiment handout, so here we only give a brief overview of the BT-7 triple-axis spectrometer [3]. The instrument (Fig. 4) has the choice of either a copper [Cu(220)] or pyrolytic graphite [PG(002)] doubly-focusing monochromator, providing a continuous incident neutron energy range from 5 to 500 meV. The 400 $cm^2$ reflecting area for each monochromator yields as much as an order-of-magnitude gain of neutrons onto the sample over earlier instruments, with available fluxes well into the $10^8$ $n/cm^2/s$ range. Generally speaking, neutron scattering is a flux-limited technique, and every experimenter wants higher count rates and better resolution. Unfortunately these are contradictory requirements, and the experimenter must carefully balance these to successfully measure the quantity of interest with sufficient resolution in the beam time available. It is therefore highly desirable to have planning tools together with a wide range of choices of instrumental parameters in order to optimize the resolution and intensity of the instrument.

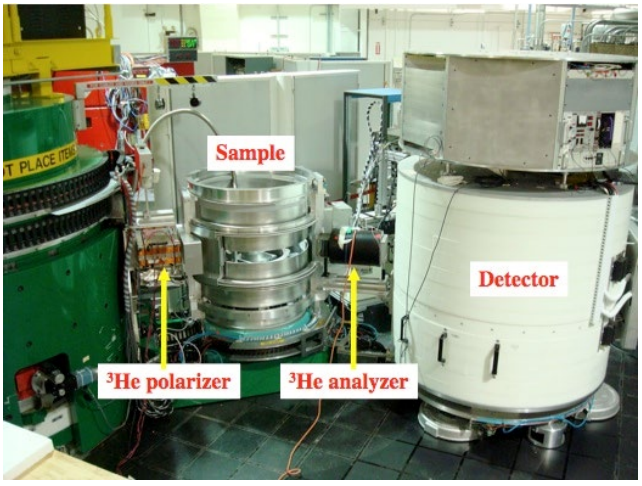


Fig. 4 The BT-7 triple-axis spectrometer with the polarized beam system installed.

The sample stage of the instrument includes two coaxial rotary tables, one for sample rotation and one for the independent rotation of magnetic field coils, and a computer controlled sample goniometer and elevator. Polarized $He^3$ cells are available to provide neutron polarization capability with either monochromator and the standard PG analyzer system.

The BT-7 analyzer system has various detectors and related collimators housed in a shield that is supported on air pads, as shown in Figs. 4, 5. The analyzer system has a multi-strip PG(002) analyzer array that can be used in a horizontally focused mode, or in a flat configuration either with a linear position-sensitive detector (PSD) or with conventional Söller collimators. All options can be selected and interchanged through the instrument control program (ICE) without any mechanical changes or user intervention. A separate diffraction detector is provided in front of the analyzer for Bragg peak

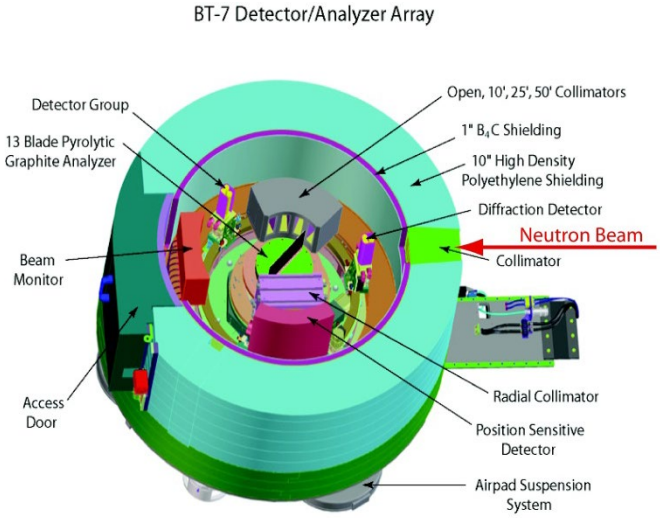


Fig. 5. Schematic of the BT-7 detector/analyzer system.

measurements, and a series of 11 detectors imbedded in the shielding behind the analyzer continuously monitor the neutron flux entering the analyzer system. These detectors can also be used for measurements of

the instantaneous correlation function, for example, or with a radial collimator to determine a diffraction pattern over a limited angular range. The PSD can also be used with a radial collimator to determine the diffraction pattern or instantaneous correlation function, with higher angular resolution.

General Specifications for BT-7:

- Velocity Selector or PG filter in reactor beam, remotely insertable.
- Double focusing PG(002) (d=3.35416 Å) or Cu(220) (d=1.273 Å) monochromator crystals
- Flat PG or horizontally focused PG (13 blades, 2 cm wide each)
- Optically pumped $He^3$ polarizers, computer controlled guide field, NMR spin rotation capability
- Monochromator take-off angles 2θ from 16 to 75 degrees
- Variable incident energy from 5.0 to 500 meV
- Scattering angles from 0 to 120 degrees
- Söller slit collimation of 10′, 25′, 50′, 80′and open at most positions.
- Radial collimators are available before and after the analyzer.
- Computer controlled vertical or horizontal guide field at sample position.

*Question: (1) What are the advantages of using a position-sensitive detector? (2) What is the best instrumental configuration if the spin-wave excitations above 40 meV were to be measured on BT-7?*

## III. EXPERIMENT AND ANALYSIS

### Simple ferromagnetic spin-waves

Perhaps one of the simplest microscopic models of magnetism starts from the Heisenberg Hamiltonian. It is generally applicable to systems in which the spins are localized on atomic sites, and where the spin interactions are mediated by direct overlap of their atomic wave-functions, or through intermediaries such as oxygen (superexchange) or through conduction electrons (indirect, or Ruderman-Kittel-Kasuya-Yosida (RKKY) exchange). The resulting magnetism originates from a combination of the Coulomb repulsion and the Pauli exclusion principle. In this model, the interaction energy between two neighboring spins is simply

$$E = -J\mathbf{S}_1 \cdot \mathbf{S}_2 \qquad (1)$$

where $J$ is the exchange constant representing the strength of magnetic exchange, and $\mathbf{S_i}$ is a vector operator of the $i^{th}$ spin. If J is positive, then a lower energy occurs when the moments are parallel, while if J is negative then the spins will align antiparallel to lower their energies. To get the total energy of the system we simply sum over all the spins in the system:

$$H = -\frac{1}{2}\sum_{i,j} \boldsymbol{J}_{i,j}\mathbf{S}_i \cdot \mathbf{S}_j \quad . \qquad (2)$$

Often the exchange for nearest-neighbor spins dominates the energetics and the ground state is either a ferromagnet (all spins parallel) or an antiferromagnetic (nearest neighbor spins antiparallel). Other types of exchange interactions can and do occur that lead to more complicated spin arrangements (See Fig. 6(a)) in many systems. Typically the exchange energies are taken as fitting parameters to be determined experimentally, and due to its simplicity this model is often used as a starting point to fit data regardless of the underlying physics of the magnetism.

*Question: where did the factor of ½ come from in Eq. (2)?*

But given the ground state of the system, how do we make a magnetic excitation? One of the simplest excitations we could imagine is to simply flip the direction of one of the spins. However, the energy cost of this would be very large (12J for a simple cubic lattice), in fact, this is the highest energy excitation you can make. A much lower energy excitation can be achieved if this single spin reversal is shared among many spins. Classically, if we allow the spins to precess about their axes, then a spin-wave can be thought of as a constant phase difference between the precession rates of neighboring spins (see Fig. 6(b)).

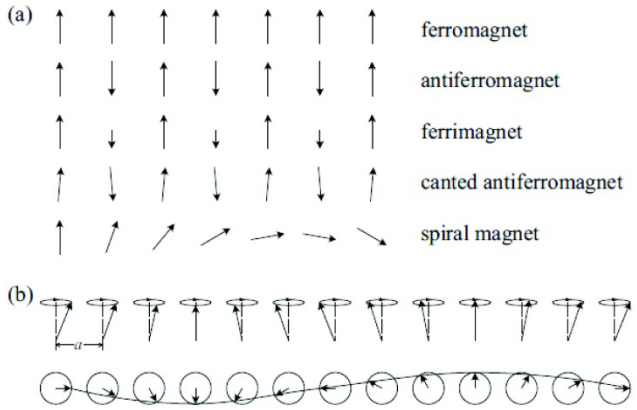


Fig. 6(a) Examples of simple magnetic ordering patterns. (b) Classical representation (side and top views) of a spin wave excitation in a one-dimensional ferromagnet.

The measured spin wave dispersion relation at low temperatures for $La_{0.85}Sr_{0.15}MnO_3$ [4], which is similar to the sample we are going to study [5], is shown in Fig. 7. We can see that the energy of the spin waves at small reduced wave vector **q** (long spin wave wavelength) is very small, while at the zone boundary, the excitation energy rises to a relatively high energy of 55 meV (short wavelength excitations mean that the excitation is shared by fewer spins and that neighboring spins are out of phase to a much greater extent, thus requiring more energy to excite). Assuming nearest-neighbor exchange only, the solution to the spin wave excitation energies for our simple Hamiltonian gives the following spin wave dispersion relation:

$$E_{SW} = 8SJ\sin^2\left(qa/2\right) \qquad (3)$$

where $a$ is the lattice parameter (nearest-neighbor distance). Because of time restrictions, we will be focusing on the small-q spin wave excitations in this experiment, where we may expand the sine function in the dispersion relation to obtain the approximate expression

$$E_{SW} = 2JSa^2q^2 \quad . \qquad (4)$$

Note that we have $E \to 0$ as $q \to 0$, which is the definition of an isotropic ferromagnet; with $q = 2\pi/\lambda$, $q$=0 corresponds to infinite wavelength, i.e. a uniform rotation of the entire spin system, which for an isotropic system costs no energy by definition (Goldstone Theorem). More generally, we should also include the possibility of magnetic anisotropy in the system, because in real spin systems the moments prefer to point along one particular crystallographic direction. This is represented by the gap parameter, Δ. This particular direction is called the magnetic easy axis, and represents the energy required to rotate the spins away from this easy direction. Then for a completely isotropic system, Δ≡0. A "soft" ferromagnet is one where Δ is small, which judging from Fig. 7 is the case for the present system. A recent example of a kagome lattice isotropic ferromagnetic is $Fe_3Sn_2$.[6] For a "hard" or "permanent" magnet, this costs a lot of energy, and Δ will be large.

*Question: What kind of magnet is your refrigerator, hard, soft, or non-magnetic?*

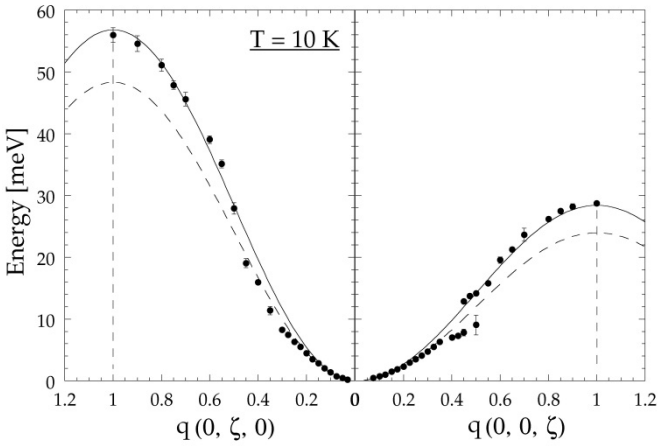


Fig. 7. Measured spin wave dispersion relations in $La_{0.85}Sr_{0.15}MnO_3$. The wave vectors are based on the orthorhombic representation for the crystal structure [4].

### Temperature Dependent Properties

For a ferromagnet, the ordered magnetic moment on each atomic site (or equivalently, the bulk magnetization) is a maximum at low T, in the ground state, while it vanishes (by definition) at the ordering temperature, $T_C$. How do we get from the state with maximum magnetization to one where it vanishes? By thermally exciting spin waves—each spin wave we create lowers the magnetization by 1 $\mu_B$. As we approach the ordering temperature, the magnetization is expected to follow a power law:

$$M(T) \propto \left( \frac{T_C - T}{T_C} \right)^{\beta} \qquad (5)$$

where the critical exponent β≈0.3 for this type of magnet.

*Question: What do you mean, "this type of magnet"? What controls the value of β?*

The magnetization, or sublattice magnetization for an antiferromagnet, can be directly determined in a neutron measurement. The integrated intensity for a magnetic Bragg reflection is given (for a simple collinear magnetic structure) by [7]

$$I = CA(\theta_B) \left\langle 1 - \left( \hat{\tau} \cdot \hat{M} \right)^2 \right\rangle |F_M|^2 \qquad (6)$$

where $\hat{\tau}$ and $\hat{M}$ are unit vectors in the direction of the reciprocal lattice vector $\boldsymbol{\tau}$ and the spin direction, **M**, respectively, and the orientation factor <…> must be evaluated for all possible domains. C includes an instrumental constant which includes the resolution of the measurement, and A(θ) is an angular factor which depends on the method of measurement. The magnetic structure factor $F_M$, is given by

$$F_M = \frac{\gamma e^2}{2mc^2} \sum_j \langle \mu_j^z \rangle f(\boldsymbol{\tau})_j e^{-W_j} e^{-i\boldsymbol{\tau} \mathbf{r}_j} \qquad (7)$$

where <…> is the thermal average of the aligned magnetic moment in Bohr magnetons of the magnetic ion at the $j^{th}$ site at position $r_j$, $W_j$ is the Debye Waller factor for the $j^{th}$ atom, f(**τ**) is the magnetic form factor (Fourier transform of the magnetization density), the neutron-electron coupling constant is $\frac{\gamma e^2}{2mc^2}$=-0.2695 $\cdot 10^{-12}$ cm, and the sum extends over all magnetic atoms in the unit cell. We see from these expressions that neutrons are sensitive to the location of magnetic atoms and the spatial distribution of their magnetic electrons; the temperature, field,... dependence of the thermal average of the ordered moment, which is directly related to the order parameter for the magnetic phase. An example of the magnetic scattering is given in Fig. 8 [8]. Note that the magnetic intensity is proportional to the square of the ordered moment.

We should also expect the spin wave spectrum to change with temperature. Mean field theory simply

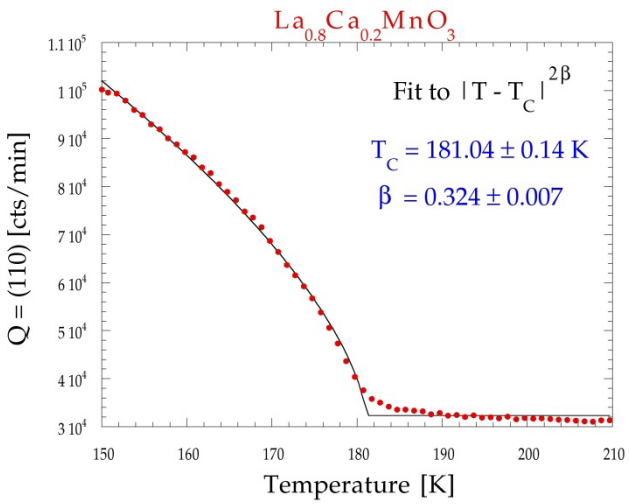


Fig. 8. Temperature dependence of the integrated intensity of the ferromagnetic (1 1 0) peak for $La_{0.8}Ca_{0.2}MnO_3$ [8].

replaces *S* with the thermal average value, which (within a constant) is the magnetization. From Eq. (3) we can then expect the spin waves to lower their energies, or renormalize, with T. Generally, we can write the spin wave dispersion relation in the small q regime as a Taylor series in q:

$$E_{spinwaves} = \Delta(T) + D(T)q^2 + E(T)q^4 + \ldots (8)$$

where *D* is the spin-wave "stiffness" parameter, and the rest of the terms are higher order terms in a Taylor expansion. The quantitative value of the stiffness parameter *D* depends on the details of the interactions and the nature of the magnetism, such as whether the magnetic electrons are localized or itinerant, or the structure is amorphous or crystalline, but the general from of the spin wave dispersion relation is the same for all isotropic ferromagnets. As T→$T_C$, *D*(T) follows M(T) in mean field theory, while more generally in the critical regime just below magnetic ordering temperature $T_C$, *D*(T) should follow a power law given by

$$D(T) \propto \left( \frac{T_C - T}{T_C} \right)^{\nu' - \beta} \qquad (9)$$

where ν′ (≈2/3) is the critical exponent for the correlation length below $T_C$. Fig. 9 shows examples of spin waves measurements, and Fig. 10 shows the renormalization of the spin waves energies with temperature.

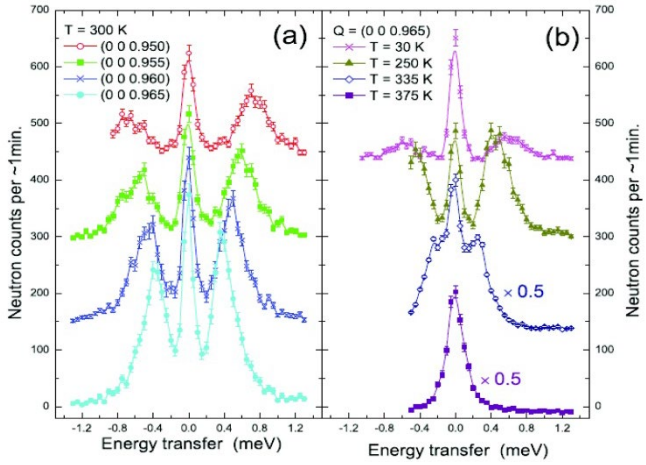


Fig. 9. Constant-Q scans revealing spin wave excitations for $La_{0.7}Sr_{0.3}MnO_3$ (a) at T = 300 K, for several wave vectors, and (b) Q = (0 0 0.965), for several temperatures [5].

At elevated temperatures, there will also be many spin waves in the system, and collisions between the spin waves will result in decays of normal modes and consequently finite intrinsic lifetimes for the spin waves. The intrinsic linewidths of the spin wave excitations in the long wavelength regime are expected to follow:

$$\Gamma(q,T) \propto q^4 \left( T \ln\left( \frac{kT}{E_{SW}} \right) \right)^2 \quad . \qquad (10)$$

Fig. 11 shows an example of spin wave linewidth measurements. Finally, we can determine the number of spin waves that are thermally populated at each energy, which is directly related to the observed intensity of the spin waves in an inelastic neutron scattering experiment. These are boson excitations (bosons are particles in which there are no restrictions on the number of particles existing in the same state), and should obey the Bose-Einstein population factor:

$$n(E_{SW}) = \frac{1}{e^{E_{SW}/kT} - 1} \quad . \qquad (11)$$

A neutron can annihilate a spin wave excitation in the sample and gain energy; the probability for this process to occur is directly proportional to the number of spin waves $n$(E) at the spin wave energy $E_{SW}$. A neutron can also create a spin wave in the system, while losing energy. The probability for this process is proportional to 1+$n$(E), where the 1 comes

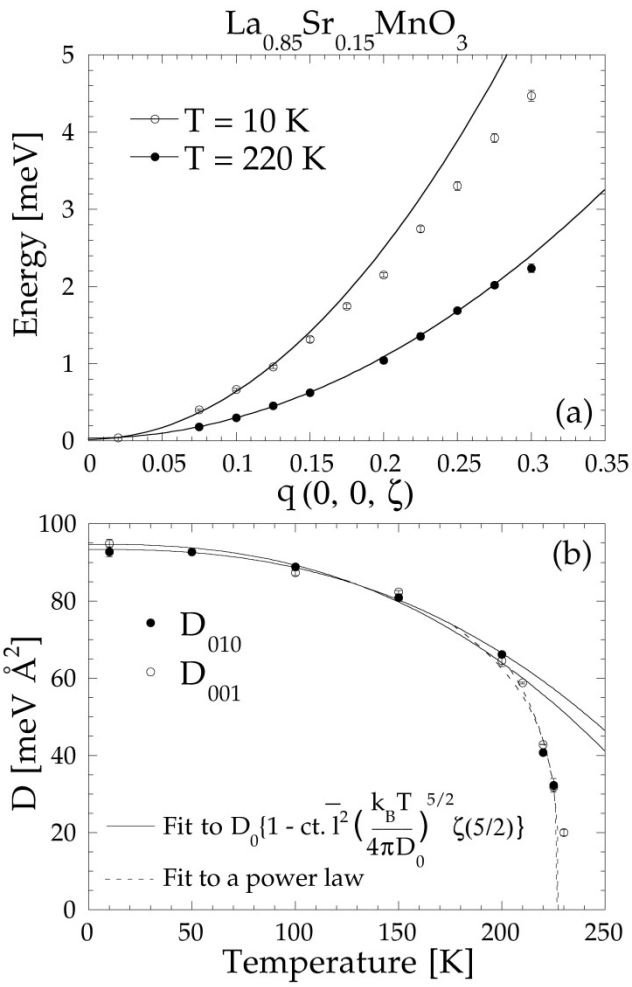


Fig. 10. (a) Low energy spin wave dispersion measured at two different temperatures and (b) the temperature dependence of the spin wave stiffness constant of $La_{0.85}Sr_{0.15}MnO_3$ [4].

from the fact that it is always possible to create a spin wave excitation, even at T = 0. This is something that we should also be able to extract from the experimental data.

**Experimental Planning and Setup**

When planning neutron scattering experiments, it is important to have as much understanding as possible of the basic properties of the material. For instance, understanding of the crystallographic information, such as lattice parameters, is imperative. In the case of single crystal samples, it is also important to have some idea about the direction of principal crystal axes. For an effective investigation, measurements of the

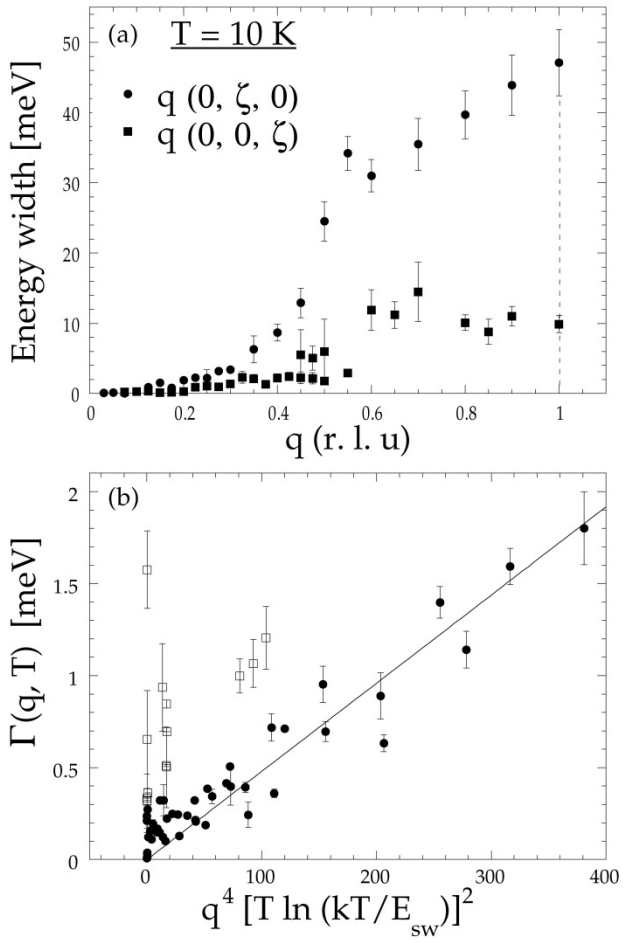


Fig. 11. Intrinsic spin wave linewidths. (a) At low temperatures there should be no intrinsic linewidth in the localized model, while the very large linewidths indicate magnon—electron damping in this metallic system. (b) At small wave vectors the linewidths follow the expected theoretical form (Eq. 10), but at larger wave vectors there are intrinsic linewidths that don't have a thermal origin [4].

bulk properties such as the magnetic susceptibility, heat capacity, and resistivity, can serve as an invaluable guide. All NCNR facility users should avail themselves of any existing data, be it their own, or published elsewhere, that could help them make more efficient use of their beam time.

Crystallographically, $La_{0.7}Sr_{0.3}MnO_3$ belongs to a space group $R\bar{3}c$ with the lattice parameters $a$=$b$=5.5084Å, $c$=13.3717Å, α=β=90°, and γ =120°. This hexagonal geometry is equivalent to a rhombohedral one with $a$=$b$=$c$=3.8835 Å and α=β=γ=90.344°. Since this is close to cubic symmetry, for convenience we will carry out the measurements based on the cubic notation.

Fig. 3(b) shows the ferromagnetic transition temperatures, $T_C$, of $La_{1-x}Sr_xMnO_3$ as a function of x. $La_{0.7}Sr_{0.3}MnO_3$ has $T_C \approx 350$ K [5]. Therefore, we need sample environment equipment that can control higher than room temperature in order to study the ferromagnetic transition.

*Question: (1) $La_{0.7}Sr_{0.3}MnO_3$ orders ferromagnetically below $T_C$ = 350 K. (1) Where in reciprocal space do we expect to find the magnetic Bragg peaks? (2) Where will the low energy spin wave excitations be located? (3) How will the spin dynamics differ between above and below $T_C$?*

The primary goal of this experiment is to measure the spin excitation spectrum in the ferromagnetically ordered phase and understand its temperature-dependent behavior. A ≈4 gram single crystal sample of $La_{0.7}Sr_{0.3}MnO_3$ has been sealed inside an aluminum container. Aluminum is among the most commonly used materials for sample containers because it is relatively transparent to neutrons, easy to machine, and is a good thermal conductor. The container has been mounted inside a He closed-cycle refrigerator/furnace that can be controlled between 30 - 600 K, and placed on top of the goniometer (or sample) table. The measurements will be done in the temperature range between 30 and 400 K.

Our measurements will proceed as follows. (Some data sets may be taken in advance and distributed.) (1) First, we will measure the integrated intensity of (1 0 0) Bragg peak as a function of temperature in the range 250-400 K. To properly obtain integrated intensities, one needs to perform both transverse (θ) and longitudinal (θ:2θ) scans. From this, we will be able to extract $T_C$ of the sample. (2) Second, we will measure the spin wave spectrum up to E ≈ 10 meV by scanning the incident energy at several Q points. From the measured data we can obtain the spin wave dispersion, which can be fit to extract the spin wave stiffness parameter, $D$(T). The spin wave data may be taken at a few selected temperatures, and the collection of data can be used to show how D changes as a function of temperature.

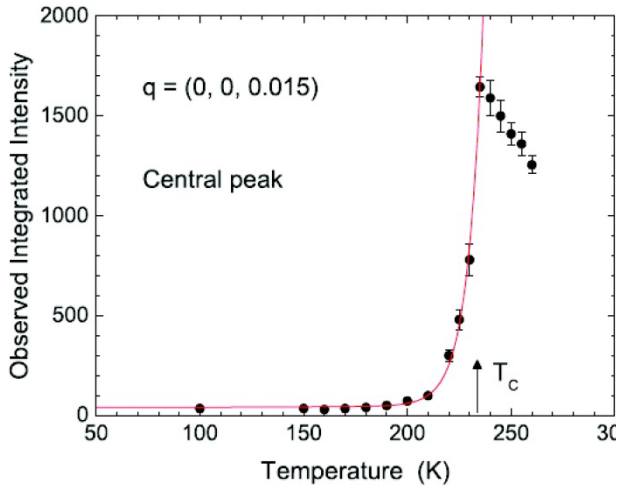


Fig. 12. Intensity of the quasielastic peak for $La_{0.85}Sr_{0.15}MnO_3$ at (0 0 1.15) as a function of temperature [4].

(3) Third, we will measure the quasielastic intensity at a certain Q close to (1 0 0) over a temperature range going through $T_C$, such as is shown in Fig. 12. The measurement will also be done by scanning the incident energy. By analyzing the integrated intensities and the linewidths of the quasielastic peaks as a function of temperature, we will be able to gain insights into the spin dynamics in the vicinity of the transition.

*Question: (1) A $\theta$ scan may show multiple peaks instead of a single Gaussian. What could be the reason if it does?*
*(2) Although it is not the case for the (1 0 0) peak in $La_{0.7}Sr_{0.3}MnO_3$, what would it mean if a $\theta$:2$\theta$ scan shows multiple peaks?*

**Data and Analysis**

Fig. 8 shows the temperature dependence of the integrated intensity of the (1 0 0) Bragg peak observed from $La_{0.8}Ca_{0.2}MnO_3$ [8]. There is an intensity increase observed below $T_C$ = 181 K, which follows a power law behavior. This intensity increase comes from ferromagnetic order on Mn sites. The sample we are going to study, $La_{0.7}Sr_{0.3}MnO_3$, will show $T_C$ at a different temperature, but the data should look similar. Knowing that spin waves are fluctuations of ordered spins around the average moment, one should expect to observe the low energy spin excitation spectrum in the vicinity of this reflection. The (1 0 0) position is particularly advantageous, since it is the smallest wave vector where ferromagnetic intensity is observed. This is because the magnetic scattering intensity generally decreases at higher momentum transfer due to the spatial distribution of unpaired electron density (magnetic form factor), as indicated in Eq. (7).

*Question: Why does the ferromagnetic peak position coincide with the nuclear peak, say, at (1 0 0)? How about antiferromagnets?*

The energy scan data we are going to obtain will be similar to what is shown in Fig. 9. Constant-Q scans typically show as many as three peaks: a central (quasi)elastic peak and an inelastic spin wave peak on each side of positive (neutron energy loss—spin wave creation) and negative (neutron energy gain—spin wave annihilation) energy transfer. Fig. 9(a) shows that the spin wave energy increases as we move away from the ferromagnetic (0 0 1) peak. The temperature dependence of $D$ is demonstrated by the data shown in Fig. 9(b). Although the lineshape of triple-axis data is a complex function of various parameters, one can approximately extract the energy values by fitting with Gaussian (if the intrinsic linewidth is small) or Lorentzian (if the intrinsic spin wave linewidth is large) functions. A series of energy values obtained at various momentum transfers can be used to obtain the dispersion relation. The dispersion relation in an isotropic ferromagnet can be conveniently expressed by Eqs. (3,4), where the temperature dependent spin stiffness constant is denoted as $D$(T). Fig. 10(a) shows results obtained from $La_{0.85}Sr_{0.15}MnO_3$ at two different temperatures, and the obtained $D$(T) is plotted in Fig. 10(b). The quantitative values of the stiffness constant $D$ depend on the details of the interactions and the nature of the magnetism, but the general form of the spin wave dispersion relation is the same for all isotropic ferromagnets.

Finally, the integrated intensities of the quasielastic central peaks are obtained and the result will be similar to what is shown in Fig. 12. These data were obtained slightly away from the ferromagnetic zone center (q=0), since otherwise the counts will be swamped by the intense nuclear and magnetic Bragg

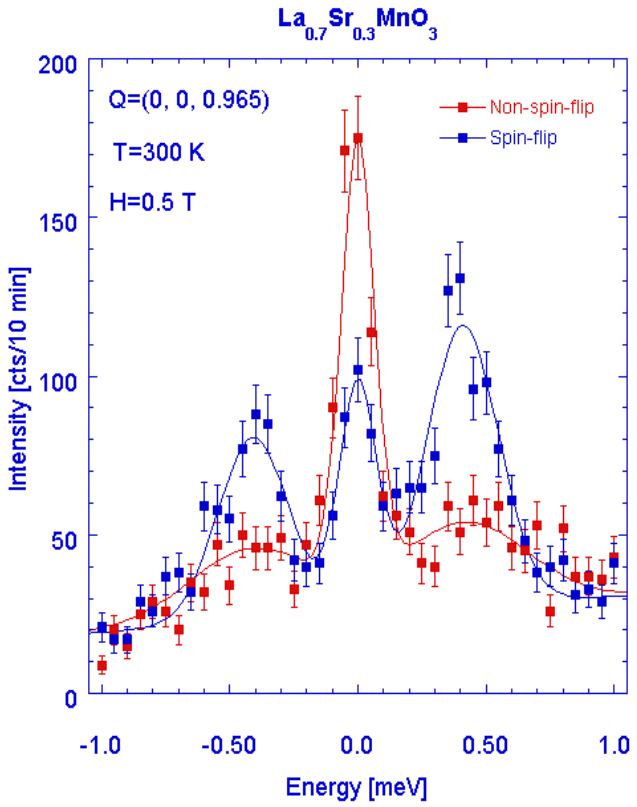


Fig. 13. An energy scan through the spin wave excitations in $La_{0.7}Sr_{0.3}MnO_3$ using polarized neutrons incident on the sample, and analyzing the polarization state of the scattered neutrons, with the neutron polarization $\mathbf{P}\perp\mathbf{Q}$. Spin wave scattering can reverse, or "flip" the neutron spin, while spin diffusion may not. The data here were taken for both spin-flip and non-spin-flip channels, and the difference in intensities shows that the inelastic signal is due to the expected spin wave scattering. The quasielastic peak in the non-spin-flip scattering is due to spin diffusion, together with an elastic (resolution-limited) peak is from magnetic clusters (polarons [8-12]) and nuclear incoherent scattering.

scattering. In the paramagnetic phase the central peak slowly gains intensity as we lower the temperature and approach $T_C$, and quickly drops in intensity below $T_C$. The intensity above $T_C$ comes from paramagnetic spin fluctuations, while that below $T_C$ it is mostly from spin waves, which quickly move to higher energies and out of the range of these quasielastic measurements. The intrinsic linewidths (Fig. 11), if available, provide a determination of the lifetimes of the magnetic excitations.

### Polarized Neutron Scattering

Finally, we remark about the use of polarized neutrons. We have previously learned that neutrons interact either with nuclei or with unpaired electrons.

While it is useful to have more than one type of neutron-sample interaction, it can also be a source of confusion. Therefore, it becomes an important issue how to discriminate magnetic scattering from nuclear scattering. There are several experimental clues to identify the origin of the scattering. Magnetic scattering follows a magnetic form factor [Eq. (7)], so the intensity decreases with increasing Q, while phonon scattering generally increases as $Q^2$. The temperature dependence also can identify whether the scattering is spin wave (qualitatively changing character above the ordering temperature) or phonon. If these trends are not definitive, however, then the most powerful and unambiguous method of neutron polarization analysis can be employed. This takes advantage of the fact that a neutron can reverse its spin direction when the origin of the scattering is magnetic (magnetic Bragg peaks, spin waves, critical scattering, etc.), while the scattering is always non-spin-flip for coherent nuclear scattering (structural Bragg peaks, phonons, etc). Since the neutron polarization analysis involves many experimental complexities and requires multiple measurements that are time consuming, we will not perform this during the school. Nevertheless, the data shown in Fig. 13, which were previously taken with this technique, powerfully confirm that the scattering we observe in $La_{0.7}Sr_{0.3}MnO_3$ is truly magnetic in nature. The present manganite class of materials continues to be under active investigation [13].

## IV. Summary

Neutron scattering can be used to make a complete determination of the magnetic properties of a system. In order of the complexity of the measurement that needs to be carried out, the magnetic order parameter is typically the easiest quantity to measure, since the scattering is strong and localized at a point in reciprocal space. The magnetic structure and spin direction(s) can be determined by measuring a series of magnetic Bragg peaks, and the magnetic form factor—Fourier transform of the magnetization density—can be determined with more effort. Inelastic scattering, on the other hand, is spread throughout the (three dimensional) Brillouin zone, and

is thus much weaker in any particular measurement and requires larger samples and considerably more effort. However, it leads to the determination of the fundamental magnetic interactions of the systems. Further effort still is needed to determine spin wave linewidths, critical scattering and exponents, and the general nature of paramagnetic fluctuations. But neutron scattering has the capability of making a complete determination of the nature and origin of the magnetism of any class of materials. The present school has focused on this magnetic system, but neutron scattering can be employed equally well in the investigation of crystal structures and lattice dynamics.

## V. References


[1] For reviews, see for example, N. Nagaosa, and Y. Tokura, Science **288**, 462 (2000); E. Dagotto, Science **309**, 257 (2005); *Nanoscale Phase Separation and Colossal Magnetoresistance*, Springer, Berlin, (2002).

[2] Insulator-metal transition and giant magnetoresistance in $La_{1-x}Sr_xMnO_3$, A. Urushibara, Y. Moritomo, T. Arima, A. Asamitsu, G. Kido, and Y. Tokura, Phys. Rev. B**51**, 14103 (1995).

[3] Double Focusing Thermal Triple Axis Spectrometer at the NCNR**,** J. W. Lynn, Y. Chen, S. Chang, Y. Zhao, S. Chi, W. Ratcliff, II, B. G. Ueland, and R. W. Erwin, Journal of Research of NIST **117**, 61-79 (2012).

[4] Structure and Spin Dynamics of $La_{0.85}Sr_{0.15}MnO_3$, Lida Vasiliu-Doloc, J. W. Lynn, A. H. Moudden, A. M. de Leon-Guevara, and A. Revcolevschi, Phys. Rev. B**58**, 14913 (1998).

[5] Spin Dynamics of Strongly Doped $La_{1-x}Sr_xMnO_3$, L. Vasiliu-Doloc, J. W. Lynn, Y. M. Mukovskii, A. A. Arsenov, and D. A. Shulyatev, J. Appl. Phys. **83**, 7342 (1998).

[6] Isotropic Nature of the Metallic Kagome Ferromagnet $Fe_3Sn_2$ at High Temperatures**,** Rebecca L. Dally, Daniel Phelan, Nicholas Bishop, Nirmal J. Ghimire and Jeffrey W. Lynn, ***Crystals* 11**, 307 (2021).

[7] Magnetic Neutron Scattering, J. W. Lynn, J. Appl. Phys. **75**, 6806 (1994); Magnetic Scattering, J. W. Lynn and B. Keimer, in *Handbook of Magnetism and Magnetic Materials*, ed. by M. Coey and S. Parkin, Springer Nature's Major Reference Work (2021).

[8] First-order Nature of the Ferromagnetic Phase Transition in (La-Ca)$MnO_3$ near optimal doping, C. P. Adams, J. W. Lynn, V. N. Smolyaninova, A. Biswas, R. L. Greene, W. Ratcliff, II, S-W. Cheong, Y. M. Mukovski, and D. A. Shulyatev, Phys. Rev. B**70**, 134414 (2004).

[9] Charge Ordering and Polaron Formation in the Magnetoresistive Oxide $La_{0.7}Ca_{0.3}MnO_3$, C. P. Adams, J. W. Lynn, Y. M. Mukovskii, A. A. Arsenov, and D. A. Shulyatev, Phys. Rev. Lett. **85**, 3954 (2000).

[10] Charge Correlations in the Magnetoresistive Oxide $La_{0.7}Ca_{0.3}MnO_3$, J. W. Lynn, C. P. Adams, Y. M. Mukovskii, A. A. Arsenov, and D. A. Shulyatev, J. Appl. Phys. **89**, 6846 (2001).

[11] Order and Dynamics of Intrinsic Nanoscale Inhomogeneities in Manganites, J. W. Lynn, D. N. Argyriou, Y. Ren, Y. Chen, Y. M. Mukovskii, and D. A. Shulyatev, *Phys. Rev.* B **76**, 014437 (2007).

[12] Polaron Formation in the Optimally Doped Ferromagnetic Manganites $La_{0.7}Sr_{0.3}MnO_3$ and $La_{0.7}Ba_{0.3}MnO_3$, Y. Chen, B. G. Ueland, J. W. Lynn, G. L. Bychkov, S. N. Barilo, and Y. M. Mukovskii, *Phys. Rev.* B **78**, 212301 (2008).

[13] See, for example, Evolution of Spin-Wave Excitations in Ferromagnetic Metallic Manganites, F. Ye, P. Dai, J. A. Fernandez-Baca, H. Sha, J. W. Lynn, H. Kawano-Furukawa, Y. Tomioka, Y. Tokura, and J. Zhang, Phys. Rev. Lett. **96**, 047204 (2006); Quantized Spin Waves in the Metallic State of Magnetoresistive Manganites, S. Petit, M. Hennion, F. Moussa, D. Lamago, A. Ivanov, Y. M. Mukovskii, and D. Shulyatev, *Phys. Rev. Lett.* **102**, 207201 (2009); Spin wave damping arising from phase coexistence below $T_C$ in colossal magnetoresistive $La_{0.7}Ca_{0.3}MnO_3$, Joel S. Helton, Susumu K. Jones, Daniel Parshall, Matthew B. Stone, Dmitry A. Shulyatev, and Jeffrey W. Lynn, *Phys. Rev.* B **96**, 104417 (2017); Damping and softening of transverse acoustic phonons in colossal magnetoresistive $La_{0.7}Ca_{0.3}MnO_3$, Joel S. Helton, Yang Zhao, Dmitry A. Shulyatev, and Jeffrey W. Lynn, *Phys. Rev.* B **99**, 024407 (2019).